lubricants

MDPI

Article

Mechanical and Tribological Properties of Ni-B and Ni-B-W Coatings Prepared by Electroless Plating

Fan Zhao, Hong Hu, Jiaxin Yu *, Jianping Lai, Hongtu He, Yafeng Zhang, Huimin Qi and Dongwei Wang

Key Laboratory of Testing Technology for Manufacturing Process in Ministry of Education, State Key Laboratory of Environment-Friendly Energy Materials, Southwest University of Science and Technology, Mianyang 621010, China
* Correspondence: yujiaxin@swust.edu.cn; Tel.: +86-816-6089708; Fax: +86-816-6089685

Abstract: Ni-B binary coating and Ni-B-W ternary coating were successfully prepared on titanium alloy (TC4) substrates by electroless plating to improve the hardness and wear resistance, followed by annealing treatment for better mechanical properties and tribological properties. The morphology, composition, microstructure, mechanical properties, and tribological behaviors of the coatings were characterized. Both as-plated coatings were amorphous, while the composition and morphology of the Ni-B-W coating differed from those of the Ni-B coating. Additionally, the Ni-B-W coating had better mechanical and tribological properties with a more considerable hardness (13.5 GPa), a minor friction coefficient (0.42), and a lower wear rate (0.10×10^{-7} $cm^3/(N \cdot m)$). After annealing, both coatings were crystalline. In parallel to the as-plated coating, the annealed coatings showed larger hardness values because of the formation of hard phases. Moreover, the crystalline grain of the coatings grew as the annealing temperature rose from 350 °C to 650 °C. Accordingly, the coatings showed a minor hardness value, a major friction coefficient, and severe wear under the same conditions. Above all, the Ni-B-W coating annealed at 350 °C showed the best performance, with an average grain size of 26.3 nm, hardness of 15.9 GPa, friction coefficient of 0.34, and wear rate of 0.09×10^{-7} $cm^3/(N \cdot m)$.

Keywords: Ni-B-W; electroless plating; annealing treatment; tribological property; wear mechanism

Citation: Zhao, F.; Hu, H.; Yu, J.; Lai, J.; He, H.; Zhang, Y.; Qi, H.; Wang, D. Mechanical and Tribological Properties of Ni-B and Ni-B-W Coatings Prepared by Electroless Plating. *Lubricants* **2023**, *11*, 42. https://doi.org/10.3390/lubricants11020042

Received: 30 November 2022
Revised: 25 December 2022
Accepted: 19 January 2023
Published: 27 January 2023

1. Introduction

Titanium alloys are widely applied in a great many fields, such as aerospace [1,2], the automotive industry [3], biomedicine [4,5], and ocean engineering [6], for their excellent properties such as low density, high strength, good biocompatibility, and corrosion resistance. However, wider applications are limited by their poor hardness and wear resistance [7,8]. The deposition of coatings by laser applications [9,10], plasma spraying [11], and a combination of electroplate and laser treatment [12] is used to improve the performance of titanium alloys [13], making great progress in terms of hardness, wear, and corrosion resistance. Additionally, other technologies such as physical vapor deposition and ultrasonic nanocrystal modification can further improve the properties of titanium alloys [14,15]. Nevertheless, the mentioned techniques are challenging for large-scale applications due to their high cost and need for professional equipment. By contrast, electroless plating has been used to acquire better surface properties with the advantages of low cost, easy operation, low equipment requirements, and deposition of uniform coatings. In particular, electroless plating has been one of the most preferred surface modification technologies for enhancing the mechanical properties and wear resistance of titanium alloys [1].

Numerous studies of electroless plated nickel-based binary alloy coatings have focused on coating preparation and performance improvement [16–20]. The study of Ni-B coatings is relatively less developed compared with that of other binary alloy coatings, such as Ni-P and Ni-Sn [17,19,21], but they have attracted much attention in the field of electroless coatings for their superior hardness and excellent wear resistance [22]. However, Ni-B

coatings are limited by their poor corrosion resistance and toughness [23]. To meet higher industrial requirements and adapt to more stringent application scenarios, multicomponent alloy coatings were invented [24]. Ni-B-P coatings are a typical example with excellent performance in terms of hardness and tribological behavior [25]. Additionally, metallic elements such as Co, Zn, Cu, Ba, Mo, and W [26–29] are commonly chosen as co-deposition elements in the preparation of Ni-B coatings. Ba co-deposition reduces the content of B in the coating, resulting in a denser structure, a larger hardness value, and better corrosion resistance [30]. Furthermore, a Ni-B-W coating was validated to possess superior corrosion resistance, good thermal stability, and a high deposition rate [31–34], indicating good prospects for aerospace, military projects, and other fields.

For instance, the microstructure of a nickel-based alloy coating was analyzed with regard to boron content, transitioning from a nanocrystalline structure to a hybrid form of nanocrystalline and amorphous with the incorporation of B. The percentage of amorphous structure was elevated with rising B content [35–43]. In contrast, an amorphous nickel-based alloy coating changes into a crystalline structure after annealing treatment, and the formation of hard phases such as Ni, Ni_2B, and Ni_3B results in larger hardness values and better wear resistance. Furthermore, with increasing annealing temperature, the grains grow and phases decompose, decreasing the hardness of the coating [44,45]. However, there has been little research about the effect of tungsten on the tribological behavior of Ni-B coatings, retarding the application process of Ni-B-W coatings.

In this paper, electroless Ni-B and Ni-B-W coatings were first plated on the surface of a titanium alloy via a new pre-treatment process and then heat-treated at different temperatures. Thereafter, the microstructural, mechanical, and tribological properties were investigated to reveal the wear mechanism of Ni-B and Ni-B-W coatings.

2. Materials and Methods

Ni-B and Ni-B-W coatings were prepared on TC4 substrate by electroless plating. The chemical composition of the substrate is given in Table 1. Titanium and its alloys have an affinity to be oxidized due to their active chemical properties, which could affect the bonding performance between coating and substrate. It is essential to eliminate the native oxide film on the surface of the substrate. Consequently, the substrate was mechanically polished with SiC papers up to 3000 grit, then cleaned ultrasonically with acetone for 8 min. Subsequently, the substrate was immersed in alkaline degreasing, acid leaching, secondary zinc leaching, and activation treatment solutions to increase the active sites on the substrate surface. After the pretreatment, the surface of the substrate was fully activated.

Table 1. The chemical composition of TC4.

Element	Ti	Al	V	Fe	C	N	H	O
Wt.%	89.82	6.12	3.97	0.05	0.01	0.01	<0.1	0.01

The substrate was immersed in electroless bath solution during the electroless plating of the Ni-B and Ni-B-W coatings. Each coating experiment took two periods of plating for 4 h in total, where the plating bath was replaced by a fresh one after the first 2 h reaction. In particular, the substrate should be cleaned with deionized water before subsequent plating to avoid pollution of the former solution. The electroless plating was carried out in a glass cell with a capacity of 100 mL, placed in a thermostatically controlled bath, where the composition of the plating bath and the operating conditions were as given in Tables 2 and 3. $NiCl_2$ and $NaBH_4$ were used as the oxidant and reductant, respectively, for both Ni-B and Ni-B-W coatings. Na_2WO_4 was used to incorporate W into the Ni-B-W coating. After the process of electroless plating, the samples were thoroughly rinsed with deionized water, dried, and kept in desiccators for characterization. A schematic diagram of the electroless plating process is shown in Figure 1.

Table 2. The electroless bath compositions of the Ni-B and Ni-B-W coatings.

Coatings	Bath Composition (g/L)					
	$NiCl_2 \cdot 6H_2O$	NaOH	$C_2H_8N_2$	$NaBH_4$	$Pb(NO_3)_2$	$Na_2WO_4 \cdot 2H_2O$
Ni-B	24.00	39.00	59.00	0.60	0.01	-
Ni-B-W	24.00	39.00	59.00	0.60	0.01	20.00

Table 3. The deposition conditions and annealing temperatures of the Ni-B and Ni-B-W coatings.

Sample No.	Deposition Conditions			Annealing Temperature (°C)
	PH	Temperature (°C)	Time (h)	
A0	13 ± 0.5	90 ± 1	2 + 2	-
A1	13 ± 0.5	90 ± 1	2 + 2	350
A2	13 ± 0.5	90 ± 1	2 + 2	500
A3	13 ± 0.5	90 ± 1	2 + 2	650
B0	13 ± 0.5	90 ± 1	2 + 2	-
B1	13 ± 0.5	90 ± 1	2 + 2	350
B2	13 ± 0.5	90 ± 1	2 + 2	500
B3	13 ± 0.5	90 ± 1	2 + 2	650

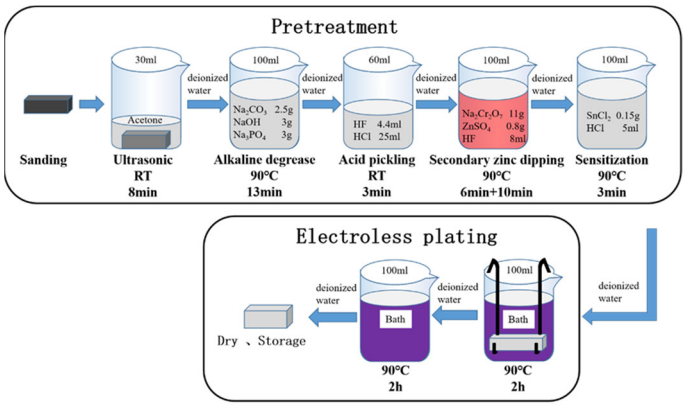

Figure 1. Schematic diagram of the electroless plating process.

Some of the deposited coatings were annealed in a muffle furnace at 350 °C, 500 °C, or 650 °C for one hour with a heating rate of 10 °C/min, followed by furnace cooling to room temperature, with the specific annealing temperatures for each sample shown in Table 3. The surface morphology and composition of the coatings were investigated by scanning electron microscope (SEM, FEI-NOVA NANOSEM 230-USA) equipped with an energy dispersive X-ray spectrometer (EDS X-MAX50). An inductively coupled plasma–optical emission spectrometer (ICP-OES, 5100, Agilent, Palo Alto, CA, USA) was used to examine the accuracy of B content measurement by EDS. Cross sections of the coatings were acquired by machining cutting and polishing to investigate the cross-sectional morphologies and thickness by optical microscope (BX51-P, Olympus, Japan). Crystalline structures and phase compositions of the coatings were identified by glancing-angle X-ray diffraction (XRD, X'Pert PRO, Holland) with Cu Kα radiation.

The hardness and elastic modulus of the coatings were obtained using a nano-indenter (G200, Keysight, Santa Rosa, CA, USA) employed with a Berkovitch diamond indenter. The maximum indentation depth was limited to less than one-tenth of the coating thickness to minimize the influence of the substrate on the results. Moreover, ten indentations were performed on each sample, and the reported hardness and elastic modulus values are the averages of the measured results. Vickers indentation was also carried out to calculate the fracture toughness (Kc) according to the formula (1) $Kc = 0.016(E/H)^{0.5} \cdot (P/c^{1.5})$. In formula (1), E and H are the elastic modulus (GPa) and nano-hardness (GPa), and P and c are the load (N) and average crack length (m) of the Vickers indentation test. The applied load was 1000 gf (10 N).

The adhesive strength of the coatings was measured using a scratch tester (MFT-4000): the maximum load was 100 N, the loading speed was 100 N/min, and the scratch velocity was 5 mm/min. The tribological behavior of the coatings was characterized using a linearly reciprocating ball-on-flat sliding tribometer (MFT3000, Rtec, San Jose, CA, USA). As for the tests of tribological behavior, Al_2O_3 balls with a diameter of 4 mm were used as the sliding counter body, the sliding distance was 3 mm, the sliding speed was 2 mm/s, the applied load was set as 20 N, and the sliding time was 30 min. Before the wear tests, the samples and Al_2O_3 balls were ultrasonically cleaned in ethanol for two minutes and dried using dry air. Each sample was subjected to three tests to ensure the reproducibility of the results. Subsequently, the wear tracks on the pieces were analyzed using white light scanning profilometry (Rtec, San Jose, CA). The wear rates (k) were calculated based on the cross-sectional profile of the wear tracks according to formula (2): $k = V/(F \cdot L)$, where F is the applied normal load (N), L is the sliding distance (m), and V is the wear volume (cm^3). Additionally, the wear volume (V) could be obtained by $V = 2\pi RS_V$ where R and S_V are the sliding track radius and worn cross-sectional area, respectively.

3. Results and Discussion

3.1. Compositions of Ni-B and Ni-B-W Coatings

Figure 2 shows the EDS results of the Ni-B and Ni-B-W coatings, which are consistent with the corresponding ICP results. Additionally, the composition of the coatings is shown in Table 4. The content of B in the Ni-B coating was 8.53 wt.%, which decreased to 7.51 wt.% in the Ni-B-W coating. Both coatings were referred to as boron-rich Ni-based coatings—a similar result to previous papers [42]. In addition, W was detected in the composition of the Ni-B-W coating, indicating that a ternary Ni-B-W coating was deposited successfully by the incorporation of Na_2WO_4 in the process of electroless plating. Besides this, the presence of O was probably due to WO_x on the surface of the coating [46].

Table 4. The compositions of the Ni-B and Ni-B-W coatings.

Coating	Wt.%			
	Ni	B	W	O
Ni-B	91.47	8.53	-	-
Ni-B-W	86.72	7.51	2.42	3.35

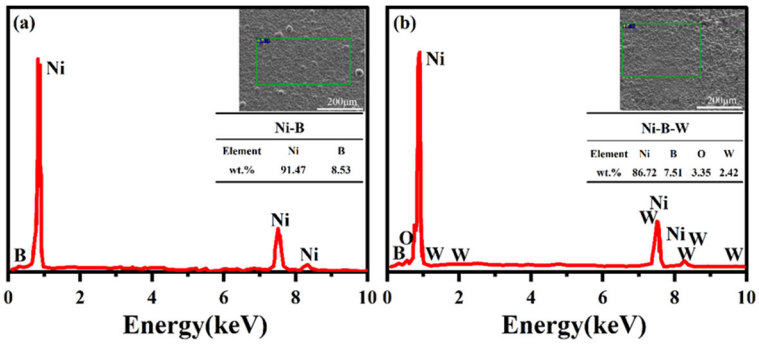

Figure 2. The EDS patterns of coatings: (**a**) A0, (**b**) B0.

3.2. Morphologies of Ni-B and Ni-B-W Coatings

Surface and cross-sectional images of the as-plated Ni-B and Ni-B-W coatings are shown in Figure 3a~d. According to Figure 3a, the Ni-B coating showed a "cauliflower" morphology, owing to the high content of B [25], while the Ni-B-W coating possessed a more compact structure, as shown in Figure 3b. Figure 3c,d shows that the thicknesses of the Ni-B and Ni-B-W coatings were about 28.6 μm and 41.3 μm, with deposition rates of 7.2 and 10.3 μm/h, respectively. Ni-B-W showed an increased deposition rate, which could

be a result of additional active sites due to the presence of W [47]. According to Figure 3e, the white light scanning results show that the surface roughness values of the Ni-B and Ni-B-W coatings were 846.8 nm and 627.3 nm respectively, indicating that W could make the coating smoother.

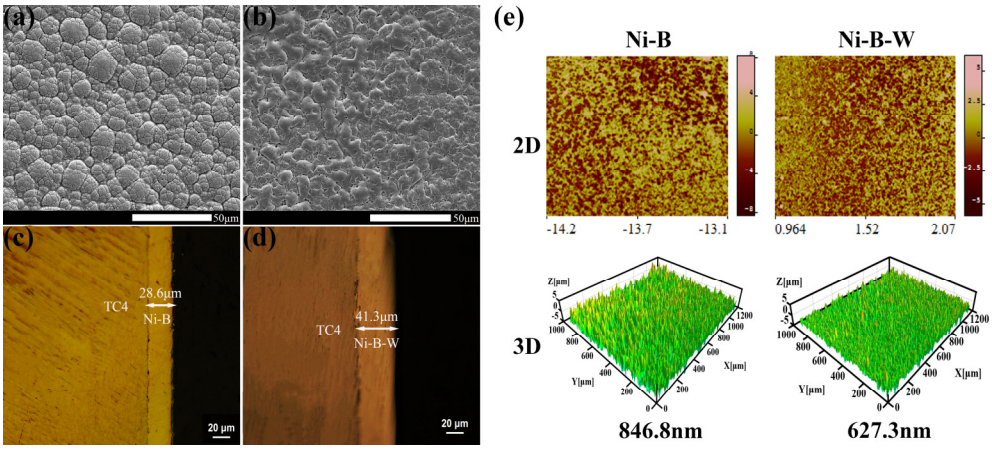

Figure 3. Surface SEM images and cross−sectional optical images of coatings: (**a**) and (**c**) A0; (**b**) and (**d**) B0. The roughness of A0 and B0 is plotted in (**e**).

Additionally, surface SEM images of the coatings annealed at different temperatures are shown in Figure 4a~f. It could be concluded that the annealed coatings showed a smother and denser surface as the annealing temperature increased [48].

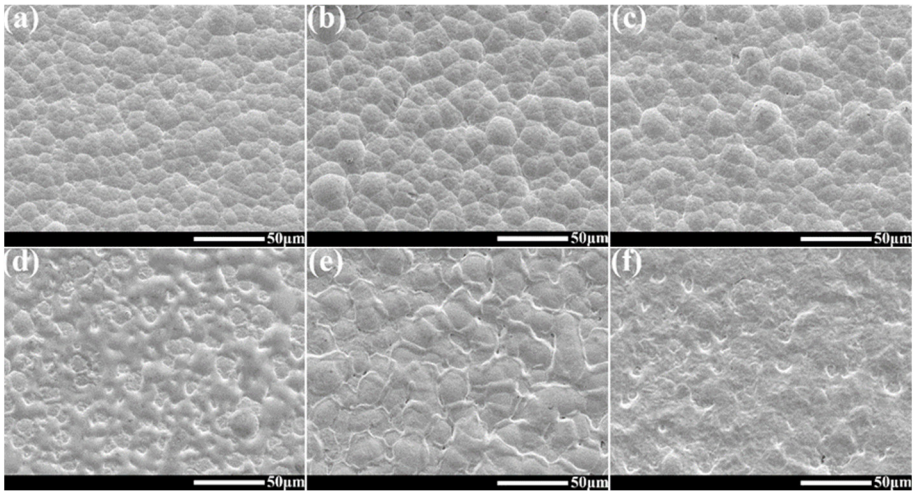

Figure 4. Surface SEM images of coatings annealed at different temperatures: (**a**) A1, (**b**) A2, (**c**) A3, (**d**) B1, (**e**) B2, (**f**) B3.

3.3. Microstructure of Ni-B and Ni-B-W Coatings

XRD was used to analyze the phases present in the coatings, as shown in Figure 5. The diffraction peaks of the as-deposited Ni-B and Ni-B-W coatings showed amorphous structures, which was related to the amorphization of Ni promoted by B and W [31,49]. In addition, both the Ni-B and Ni-B-W coatings annealed at different temperatures showed crystallization. The diffraction peaks of the Ni-B coating annealed at 350 °C were identified as those of Ni, Ni_3B, and Ni_2B phases, while the metastable Ni_2B phase disappeared in the coatings annealed at 500 and 650 °C. Likewise, Ni and Ni_3B phases were identified in the diffraction peaks of the Ni-B-W coating annealed at 350 °C. Meanwhile, the Ni_2B phase was detected and then disappeared at 500 °C and 650 °C, respectively.

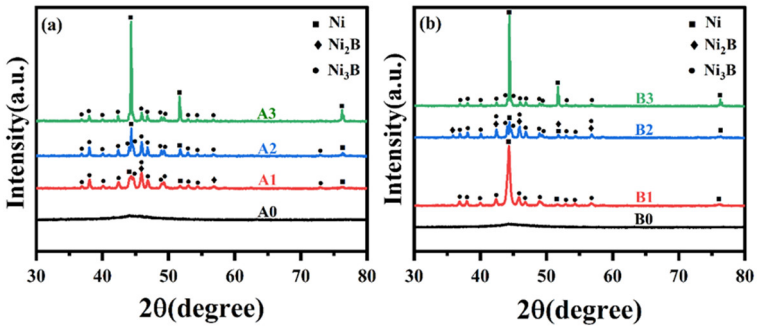

Figure 5. The XRD patterns of coatings as-plated and annealed: (**a**) Ni-B, (**b**) Ni-B-W.

Above all, the metastable Ni_2B phase appeared at a higher temperature in Ni-B-W coatings, which indicated that Ni-B-W coatings had better thermal stability [31]. Besides this, the diffraction peaks of annealed Ni-B-W coatings were shifted slightly compared with the standard peak of Ni (PDF#70-1849). Combined with the fact that W atoms with larger radii dissolve well in the crystal structure of Ni, it could be concluded that the Ni in these coatings should possess a solid solution structure [48]. Moreover, the XRD peaks of Ni-B and Ni-B-W became sharper with rising annealing temperature, which is related to the development of grains.

Additionally, the XRD results were analyzed quantitatively as follows. The averaged grain size, crystallization, and phase composition of the annealed coatings were calculated as shown in Figure 6. The average grain sizes of the Ni-B and Ni-B-W coatings changed from 32.3 nm and 26.3 nm, respectively, to 90.1 nm and 91.1 nm, respectively. Meanwhile, the crystallinity of the Ni-B and Ni-B-W coatings changed from 88.74% and 80.11%, respectively, to 93.58% to 96.4%, respectively, with increasing annealing temperature from 350 °C to 650 °C, as shown in Figure 6a,b. Likewise, the phase compositions of the Ni-B and Ni-B-W coatings are summarized in Figure 6c. It can be seen that the contents of Ni, Ni_2B, and Ni_3B phases largely depended on the annealing temperature, which was probably correlated to the transformation of the metastable Ni_2B phase [45].

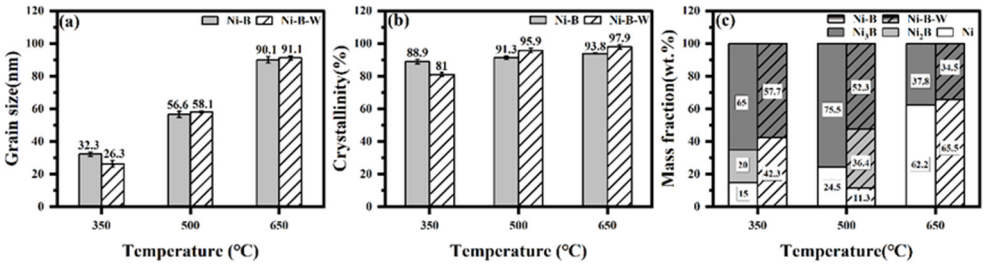

Figure 6. The characteristics of crystallization of electroless Ni-B and Ni-B-W coatings annealed at different temperatures: (**a**) grain size, (**b**) crystallinity, (**c**) mass fraction.

3.4. Mechanical Properties of Ni-B and Ni-B-W Coatings

The nano-hardness values of TC4 alloy and the coatings are shown in Figure 7. The hardness of the coatings was raised compared with that of the substrate, which illustrated that TC4 alloys (3.7 Gpa) were strengthened by electroless plating with Ni-B (7.1 Gpa) and Ni-B-W (13.5 Gpa) coatings. Additionally, the Ni-B-W coating possessed an increased hardness value compared to the Ni-B coating under the same conditions, which should be due to the presence of W [50]. The hardness of the coatings first increased at a lower annealing temperature, which was probably due to the crystallization and solution strengthening by Ni-W. Then, the hardness decreased with the rising of the annealing temperature, likely resulting from the grain growth and hard phase (Ni_3B) reduction, as shown in Figure 6c, since Ni_3B has a similar structure to cementite, which possesses high hardness [47,51].

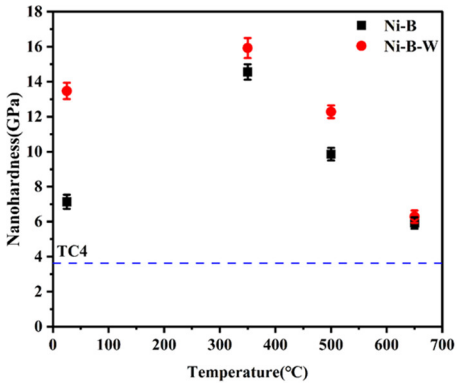

Figure 7. The nano-hardness of electroless Ni-B and Ni-B-W coatings.

Meanwhile, the fracture toughness of the coatings was calculated according to equation (1), as shown in Table 5. The fracture toughness of the B0 coating increased to 109% that of the A0 coating, with a value of 3.1 MPa·m$^{0.5}$; additionally, coatings A1, A2, and A3 and coatings B1, B2, and B3 had higher fracture toughness than A0 and B0, respectively, which indicated that W addition and heat treatment could improve the fracture toughness of electroless nickel-based coatings. Afterward, there were long cracks at the four top corners of the indentation of the A0 coating, while the cracks in the B0 coating were shorter and could only be found at high magnification, as shown in Figure 8. Furthermore, a crack was deflected in the B0 coating according to Figure 8b, having been blocked by hard particles such as Ni-W solid solution. Consequently, the stress was released and the propagation of cracks was terminated, thus toughening the coating [52].

Table 5. The fracture toughness of Ni-B and Ni-B-W coatings.

Sample	Nanohardness H (GPa)	Modulus of Elasticity E (Gpa)	Load P (N)	Average Crack Length c ($\times 10^{-5}$m)	Fracture Toughness Kc (Mpa·m$^{0.5}$)
A0	7.1	106.2	10	3.7	2.8
A1	14.6	109.8	10	2.8	2.9
A2	9.9	113.5	10	2.3	5.0
A3	5.9	110.1	10	2.2	6.9
B0	13.5	72.1	10	2.5	3.1
B1	15.9	82.6	10	2.3	3.3
B2	12.3	80.3	10	2.2	3.9
B3	6.3	78.7	10	2.1	6.1

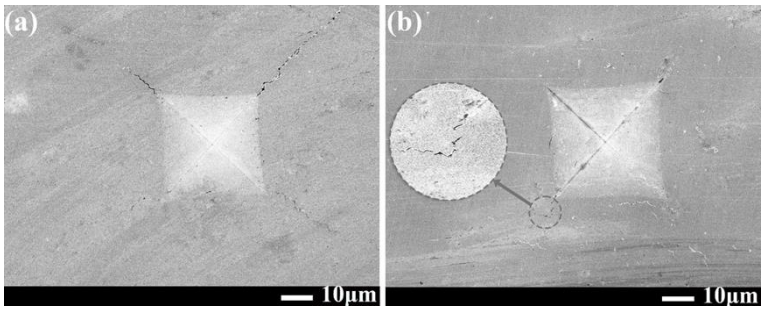

Figure 8. SEM images of Vickers indentation on polished coating surfaces: (**a**) A0, (**b**) B0.

The fracture toughness of the coatings was verified by adhesion scratch tests, as shown in Figure 9. In our study, LC2 was used to describe the adhesive strength of the Ni-B and Ni-B-W coatings, representing the load where the first chipping was observed at the edges of the scratch. The acoustic emission signals gave the same results. The adhesion of the

Ni-B-W coatings was higher than that of the Ni-B coatings and increased with the annealing temperature, showing a similar regularity with the former results.

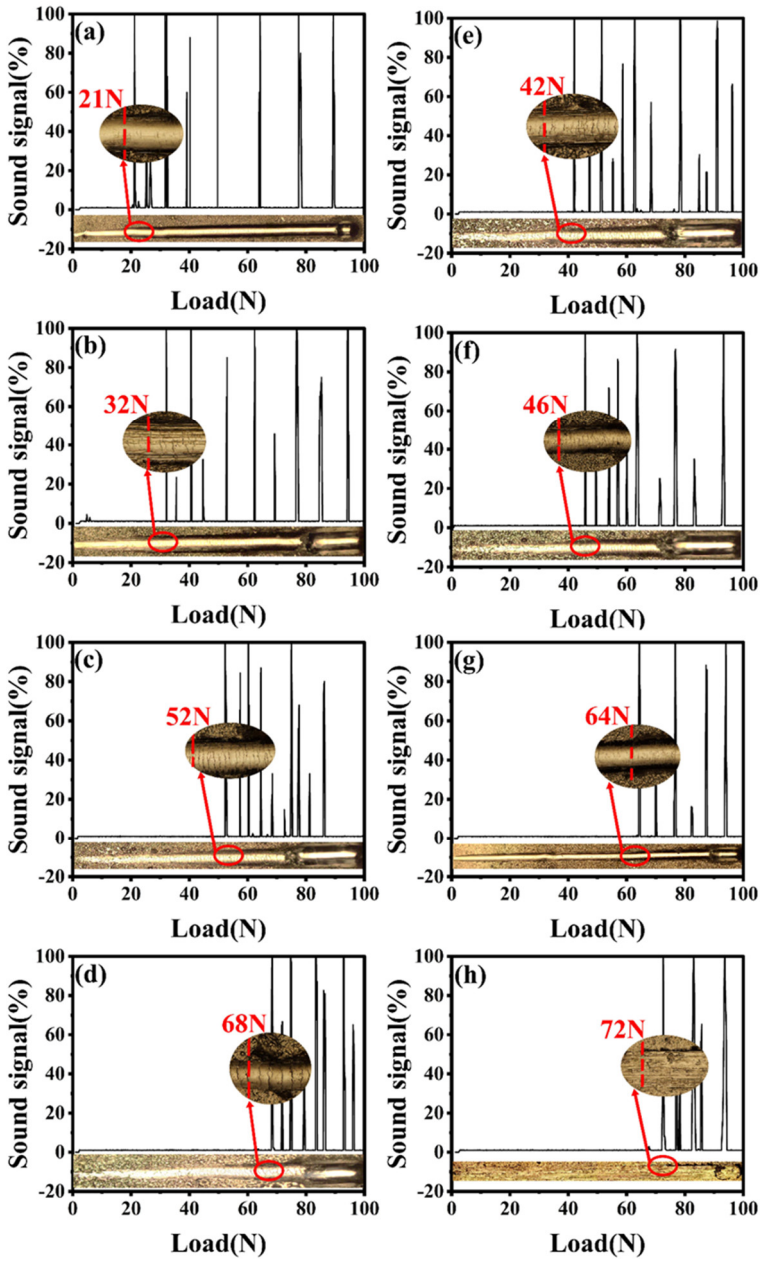

Figure 9. Sound signals and optical images of scratches in the adhesion test: (**a**) A0, (**b**) A1, (**c**) A2, (**d**) A3, (**e**) B0, (**f**) B1, (**g**) B2, (**h**) B3.

3.5. Tribological Properties of Ni−B and N−B−W Coatings

The friction coefficient of TC4 shows an unstable state throughout the whole process. The annealed Ni-B and Ni-B-W coatings entered a regular wear stage more quickly during the tribological tests than did the as-deposited coatings, as shown in Figure 10, which may be related to the low hardness and easy adhesion to the friction pair ball. Increased stability of the friction process and lower friction coefficient were observed in the Ni-B-W coatings compared to the Ni-B coatings, as shown in Figure 10b,c. For example, the friction coefficients decreased from 0.49 for A0 to 0.4 for B0, which was observed as an improvement in coating peeling due to the rising toughness. Furthermore, the friction coefficients of the annealed coatings increased and then decreased with increasing annealing temperature.

Hard phases, such as Ni, Ni_2B, and Ni_3B, formed after the annealing treatment, making the friction pair (Al_2O_3) difficult to embed into the coatings [45]. Additionally, the existence of these hard phases enhanced the ability of the coatings to resist plastic deformation, so the friction coefficient of the annealed coatings was smaller than that of the deposited ones [53].

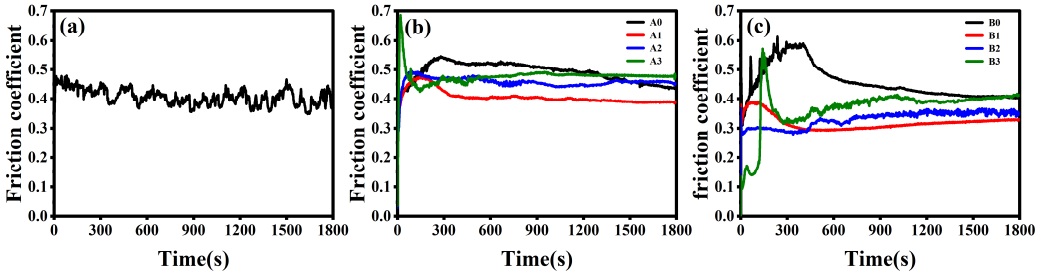

Figure 10. Profiles of the coefficient of friction: (**a**) TC4, (**b**) A0-A3, (**c**) B0-B3.

Additionally, the wear rates of the coatings were calculated and are shown in Figure 11b according to the cross-sectional profiles shown in Figure 11a. Compared with the TC4 substrate, the wear rates of electroless coatings A0 and B0 decreased by 35.4% and 99.5%, respectively. The wear rate of the B0 coating decreased to 8% that of the A0 coating, with a value of 0.10×10^{-7} $cm^3/(N{\cdot}m)$, which was attributed to the improved hardness and fracture toughness due to the presence of W. As the annealing temperature increased, the wear rates of the coatings decreased then increased with the lowest wear rate for coatings A1 and B1, with values of 0.16×10^{-7} and 0.09×10^{-7} $cm^3/(N{\cdot}m)$, respectively.

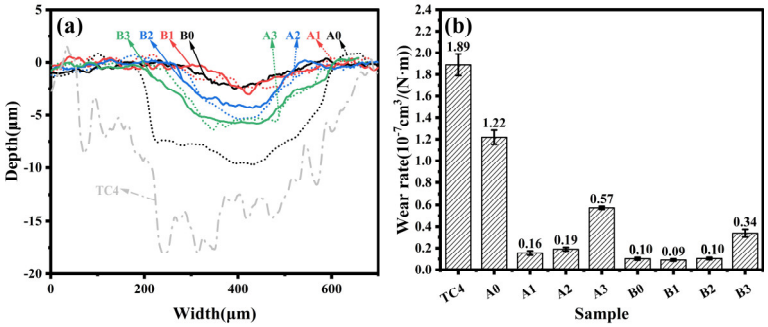

Figure 11. The cross−sectional profiles of wear tracks and the corresponding wear rates of the TC4 and coatings: (**a**) the cross−sectional profile lines; (**b**) the wear rates.

3.6. Wear Mechanism of Ni-B and Ni- B-W Coatings

Further investigations, such as the morphology and element composition inside the wear trace, were undertaken to explore the wear mechanism of the Ni-B and Ni-B-W coatings. The wear trace morphology of A0 and B0 coting were shown in Figure 12. The wear scar morphology of the A0 coating was relatively smooth, as can be seen in Figure 12a. Grooves, pits, and scaly wear scars were found at a larger magnification, as shown in Figure 12b,c. The scaly morphology is a typical appearance of abrasive wear, a plastic deformation pattern caused by stress concentration during the period of wear. Consequently, it could be concluded that coating A0 showed the form of moderate abrasive wear. In addition, adhesive and oxidation wear occurred in A0, which is supported by the presence of oxygen and aluminum according to the EDS results, as shown in Figure 12d. By contrast, the grooves in B0 were smaller and shallower, and the contents of Al and O in the wear scar were a little lower compared to those in A0, as shown in Figure 12e,f,g,h, respectively. Therefore, the wear forms of the Ni-B-W coating included slight abrasive wear, adhesive wear, and oxidation wear.

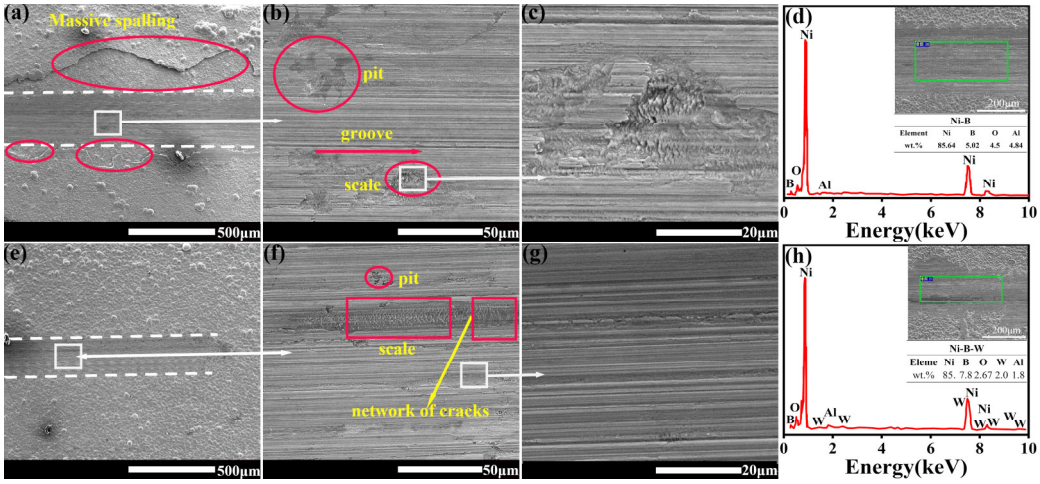

Figure 12. SEM images and EDS patterns inside the wear tracks of coatings: (**a**–**d**) A0, (**e**–**h**) B0.

Above all, it was revealed that the presence of W reduced the friction coefficient and the brittleness of the Ni-B coating. The Ni-B-W coating also possessed higher hardness and better fracture toughness to reduce the pressed depth of the abrasive particles and resist deformation during the process of the wear test. As a result, Ni-B-W showed a slight wear morphology. Consequently, the Ni-B-W coating showed a smaller wear rate than did the Ni-B coating.

The wear scar morphologies of both the Ni-B and Ni-B-W coatings annealed at different temperatures are shown in Figure 13. As for Ni-B coatings, a slight scratch of the cell body occurred on the surface of the A1 coating, according to Figure 13a, which revealed the mechanism of slight abrasive wear. With increasing annealing temperature, the cell body was completely worn out for the A2 coating, showing a scaly morphology with a few shallow pits, as shown in Figure 13b; this indicated a combination of slight adhesion and adhesive wear during the wear process. The hardness of the coatings decreased with the annealing temperature; thus, the friction pair ball could embed into the coatings more easily, leading to coating spallation as shown in Figure 13c. Ni-B-W coatings presented a similar wear pattern to Ni-B coatings as the annealing temperature increased.

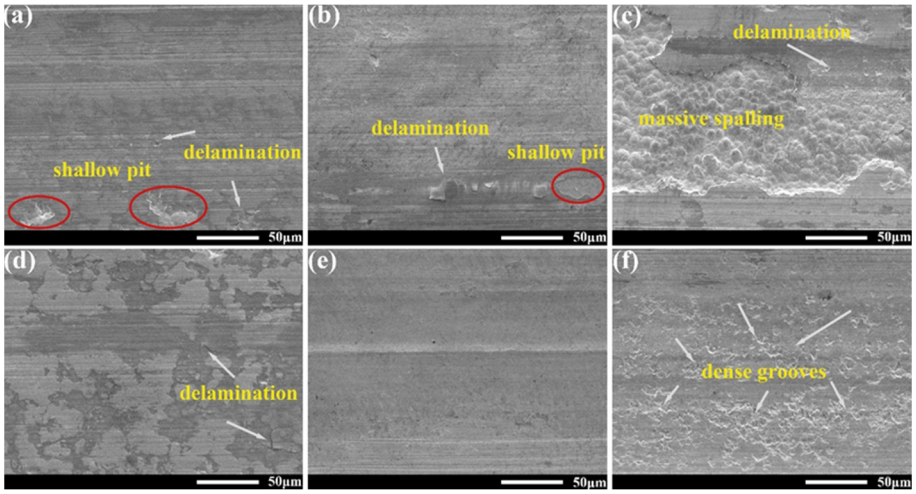

Figure 13. SEM images inside the wear tracks of coatings: (**a**) A1, (**b**) A2, (**c**) A3, (**d**) B1, (**e**) B2, (**f**) B3.

The microstructure of the annealed coatings changed from amorphous to crystalline structure, and the mechanical properties of the coatings were greatly improved, thus improving the wear resistance of the coating. Nevertheless, with the increase in annealing temperature, the grain size increased, decreasing the coating hardness [46]. Consequently,

the wear of the coating was more serious during the tribological tests, resulting in an increased friction coefficient, more small pits, and a larger area of material peeling, which aggravated the wear and significantly reduced the wear resistance.

4. Conclusions

Ni-B and Ni-B-W coatings were successfully deposited on TC4 alloy substrates by electroless plating. The as-deposited Ni-B and Ni-B-W coatings were amorphous and possessed increased hardness values compared with the substrates. The W content in the Ni-B-W ternary coating was 2.42 wt.%, and its hardness, fracture toughness, and adhesion were increased by 20.5%, 8.9%, and 70.4%, respectively, compared to those of the Ni-B coating. Additionally, the friction coefficient and wear rate of the Ni-B-W coating were decreased by 18.4% and 91.8%. Furthermore, the deposited amorphous coatings turned into crystal coatings after one hour of annealing at 350, 500, and 650 °C, with the best performance observed after the heat treatment at 350 °C. The friction coefficient of the annealed coatings increased with the annealing temperature, while the wear rate increased first and then decreased for the Ni-B and Ni-B-W coatings. Both the Ni-B and Ni-B-W coatings showed a hybrid wear form of abrasive, adhesive, and oxidation.

Author Contributions: Conceptualization, F.Z. and J.Y.; validation, F.Z. and H.H. (Hong Hu); formal analysis, H.H. (Hong Hu); investigation, F.Z. and H.H. (Hong Hu); resources, Y.Z.; data curation, H.H. (Hongtu He) and H.Q.; writing—original draft preparation, F.Z. and H.H. (Hong Hu); writing—review and editing, F.Z. and D.W.; visualization, J.L.; supervision, J.Y.; project administration, F.Z.; funding acquisition, J.Y. All authors have read and agreed to the published version of the manuscript.

Funding: This work was supported by Sichuan Science and Technology Program [2018JY0245].

Data Availability Statement: The authors confirm that the data supporting the findings of this study are available within the article.

Acknowledgments: Analysis Center, Southwest University of Science and Technology should be acknowledged in this research article for SEM, EDS, and XRD tests.

Conflicts of Interest: We declare that we have no financial and personal relationships with other people or organizations that can inappropriately influence our work, and there is no professional or other personal interest of any nature or kind in any product, service, and/or company that could be construed as influencing the position presented in, or the review of, the manuscript entitled "Mechanical and Tribological Properties of Ni-B and Ni-B-W Coatings Prepared by Electroless Plating". The funders had no role in the design of the study; in the collection, analyses, or interpretation of data; in the writing of the manuscript; or in the decision to publish the results.

References

1. Boyer, R.R. An overview on the use of titanium in the aerospace industry. *Mater. Sci. Eng. A* **1996**, *213*, 103–114. [CrossRef]
2. Zhao, Q.; Sun, Q.; Xin, S.; Chen, Y.; Wu, C.; Wang, H.; Xu, J.; Wan, M.; Zeng, W.; Zhao, Y. High-strength titanium alloys for aerospace engineering applications: A review on melting-forging process. *Mater. Sci. Eng. A* **2022**, *845*, 143260. [CrossRef]
3. Behera, A.; Sahoo, A.K.; Mohapatra, S.S. 14-Nickel-titanium smart hybrid materials for automotive industry. In *Nickel-Titanium Smart Hybrid Materials*; Elsevier: Amsterdam, The Netherlands, 2022; pp. 271–295.
4. Cai, Z.; Chen, J.; Zhang, Z.; Li, K.; Yang, X.; Xie, G. Microstructure regulation of titanium-oxygen alloy with high strength and excellent ductility for biomedical applications. *Intermetallics* **2022**, *148*, 107648. [CrossRef]
5. Chirico, C.; Romero, A.V.; Gordo, E.; Tsipas, S.A. Improvement of wear resistance of low-cost powder metallurgy β-titanium alloys for biomedical applications. *Surf. Coat. Technol.* **2022**, *434*, 128207. [CrossRef]
6. Cheng, J.; Li, F.; Zhu, S.; Yu, Y.; Qiao, Z.; Yang, J. Electrochemical corrosion and tribological evaluation of TiAl alloy for marine application. *Tribol. Int.* **2017**, *115*, 483–492. [CrossRef]
7. Zhao, Y.; Fan, Z.; Tan, Q.; Yin, Y.; Lu, M.; Huang, H. Interfacial and tribological properties of laser deposited TiOxNy/Ti composite coating on Ti alloy. *Tribol. Int.* **2021**, *155*, 106758. [CrossRef]
8. Yuan, S.; Lin, N.; Zou, J.; Lin, X.; Liu, Z.; Yu, Y.; Wang, Z.; Zeng, Q.; Chen, W.; Tian, L.; et al. In-situ fabrication of gradient titanium oxide ceramic coating on laser surface textured Ti6Al4V alloy with improved mechanical property and wear performance. *Vacuum* **2020**, *176*, 109327. [CrossRef]
9. Liu, X.; Meng, X.; Liu, H.; Shi, G.; Wu, S.; Sun, C.; Wang, M.; Qi, L. Development and characterization of laser clad high temperature self-lubricating wear resistant composite coatings on Ti-6Al-4V alloy. *Mater. Des.* **2014**, *55*, 404–409. [CrossRef]

10. Zhou, Y.; Wang, K.; Sun, Z.; Xin, R. Simultaneous improvement of strength and elongation of laser melting deposited Ti-6Al-4V titanium alloy through three-stage heat treatment. *J. Mater. Process. Technol.* **2022**, *306*, 117607. [CrossRef]
11. Feng, J.; Wang, J.; Yang, K.; Rong, J. Microstructure and performance of YTaO4 coating deposited by atmospheric plasma spraying on TC4 titanium alloy surface. *Surf. Coat. Technol.* **2022**, *431*, 128004. [CrossRef]
12. Li, Y.L.; Wu, Y.Y.; Wang, W.Q.; Lei, M.; Li, X.W. Microstructure and mechanical properties of the Ni-B-Ti composite coating on TA2 prepared by pre-plating and laser remelting. *Surf. Coat. Technol.* **2021**, *405*, 126567. [CrossRef]
13. Zhang, L.C.; Chen, L.Y.; Wang, L.Q. Surface modification of titanium and titanium alloys: Technologies, developments, and future interests. *Adv. Eng. Mater.* **2020**, *22*, 1901258. [CrossRef]
14. Koshuro, V.; Fomina, M.; Zakharevich, A.; Fomin, A. Superhard Ta-O-N coatings produced on titanium using induction physical vapor deposition. *Ceram. Int.* **2022**, *48*, 19467–19483. [CrossRef]
15. Liu, R.; Yuan, S.; Lin, N.; Zeng, Q.; Wang, Z.; Wu, Y. Application of ultrasonic nanocrystal surface modification (UNSM) technique for surface strengthening of titanium and titanium alloys: A mini review. *J. Mater. Res. Technol.* **2021**, *11*, 351–377. [CrossRef]
16. Zhang, B. Chapter 1—History-from the discovery of electroless plating to the present. In *Amorphous and Nano Alloys Electroless Depositions*; Elsevier: Oxford, UK, 2016; pp. 3–48.
17. Gunji, T.; Umehashi, Y.; Tsunoi, H.; Yokoi, K.; Kawai, A.; Matsumoto, F. Preparation of chemical-resistant atomically ordered Sn-Ni alloy films by electroless plating. *J. Alloy. Compd.* **2021**, *877*, 160100. [CrossRef]
18. Hamid, Z.A.; Hassan, H.B.; Attyia, A.M. Influence of deposition temperature and heat treatment on the performance of electroless Ni-B films. *Surf. Coat. Technol.* **2010**, *205*, 2348–2354. [CrossRef]
19. Samanta, S.; Mondal, K.; Dutta, M.; Singh, S.B. Electroless NiP coatings over API X70 steel: Effect of composition on the H-permeation and corrosion resistance. *Surf. Coat. Technol.* **2021**, *409*, 126928. [CrossRef]
20. Kaliaraj, G.S.; Vishwakarma, V.; Dawn, S.S.; Karthik, A.; Vigneshwaran, S.; Naidu, G.D. Reduction of sulphate reducing bacterial survival by Cu-Ni, Zn-Ni and Cu-Zn-Ni coatings using electroless plating technique for oil/diesel pipeline applications. *Mater. Today Proc.* **2021**, *45*, 6804–6806. [CrossRef]
21. Ma, L.; Chen, Y.; Renner, P.; Parkinson, D.; Fang, A.; Liang, H. Synthesis and Morphological Characterization of Electroless-Deposited Ni-P Coatings on Diamond Abrasives. *Lubricants* **2021**, *9*, 20. [CrossRef]
22. Pal, S.; Jayaram, V. Effect of microstructure on the hardness and dry sliding behavior of electroless Ni–B coating. *Materialia* **2018**, *4*, 47–64. [CrossRef]
23. Vitry, V.; Hastir, J.; Mégret, A.; Yazdani, S.; Yunacti, M.; Bonin, L. Recent advances in electroless nickel-boron coatings. *Surf. Coat. Technol.* **2022**, *429*, 127937. [CrossRef]
24. Yildiz, R.A.; Göksenli, A.; Yüksel, B.H.; Muhaffel, F.; Aydeniz, A. Effect of annealing temperature on the corrosion resistance of electroless produced Ni-B-W coatings. *Adv. Mater. Res.* **2013**, *2249*, 651. [CrossRef]
25. Algul, H.; Uysal, M.; Alp, A. A comparative study on morphological, mechanical and tribological properties of electroless NiP, NiB and NiBP coatings. *Appl. Surf. Sci. Adv.* **2021**, *4*, 100089. [CrossRef]
26. Ranganatha, S.; Venkatesha, T.V.; Vathsala, K. Development of electroless Ni-Zn-P/nano-TiO2 composite coatings and their properties. *Appl. Surf. Sci.* **2010**, *256*, 7377–7383. [CrossRef]
27. Valova, E.; Armyanov, S.; Hristova, G.; Vassilev, T.; Steenhaut, O.; Dille, J.; Hubin, A.; Vandendael, I. Electroless deposited Ni-Ce-P coatings. *Surf. Coat. Technol.* **2016**, *304*, 468–475. [CrossRef]
28. Zhu, L.; Luo, L.; Luo, J.; Wu, Y.; Li, J. Effect of electroless plating Ni-Cu-P layer on brazability of cemented carbide to steel. *Surf. Coat. Technol.* **2012**, *206*, 2521–2524. [CrossRef]
29. Zuxiao, Y.U.; Jian, C.; Shixiong, H.A.O.; Xiaoli, T. Study of process for electoless plating of Ni-Co-P alloy coating. *J. Mater. Prot.* **2007**, *40*, 22–24.
30. Rahmani, S.; Omrani, A.; Hosseini, S.R. Impact of barium in improving corrosion resistance and properties of electroless Ni-Ba-B alloy deposits. *Met. Mater. Int.* **2020**, *26*, 979–988. [CrossRef]
31. Mukhopadhyay, A.; Barman, T.K.; Sahoo, P. Wear and friction characteristics of electroless Ni-B-W coatings at different operating temperatures. *Mater. Res. Express* **2018**, *5*, 026526. [CrossRef]
32. Mukhopadhyay, A.; Barman, T.K.; Sahoo, P. Corrosion resistance of electroless Ni-B-W-Mo coatings using electrochemical impedance spectroscopy. *Port. Electrochim. Acta* **2019**, *37*, 193–203. [CrossRef]
33. Liu, J.; Zhang, T.; Zhang, Y.; Shao, Y.; Meng, G.; Wang, F. Friction, wear and corrosion resistance of multi-layer electroless Ni-W-P coating on AZ91D magnesium alloy. *China Surf. Eng.* **2019**, *32*, 53–62.
34. Palaniappa, M.; Seshadri, S.K. Friction and wear behavior of electroless Ni-P and Ni-W-P alloy coatings. *Wear* **2008**, *265*, 735–740. [CrossRef]
35. Bulbul, F. The effects of deposition parameters on surface morphology and crystallographic orientation of electroless Ni-B coatings. *Met. Mater. Int.* **2011**, *17*, 67–75. [CrossRef]
36. Celik, I.; Karakan, M.; Bulbul, F. Investigation of structural and tribological properties of electroless Ni-B coated pure titanium. *Proc. Inst. Mech. Eng. Part J-J. Eng. Tribol.* **2016**, *230*, 57–63. [CrossRef]
37. Cheng, X.; Rao, Q. A study of microstructure of electroless nickel-boron alloy coatings. *Electroplat. Pollut. Control* **2012**, *32*, 19–21.
38. Das, S.K.; Sahoo, P. Influence of process parameters on microhardness of electroless Ni-B coatings. *Adv. Mech. Eng.* **2012**, *4*, 703168. [CrossRef]

39. Pan, J.; Chen, R.; Wu, C. Research on micro-structure of electroless Ni-B coatings. In Proceedings of the 2nd International Conference on Materials and Products Manufacturing Technology, Guangzhou, China, 22–23 September 2012; pp. 1641–1645.
40. Qian, W.; Chen, H.; Feng, C.; Zhu, L.; Wei, H.; Han, S.; Li, G.; Lin, H.; Jiang, J. Microstructure and properties of the Ni-B and Ni-B-Ce ultrasonic-assisted electroless coatings. *Surf. Rev. Lett.* **2018**, *25*, 1950006. [CrossRef]
41. Rao, Q.; Wang, H.; Fan, X.; Zhou, Y. Morphology and formation mechanism of electroless Ni-B alloy coating. *J. Shanghai Jiaotong Univ.* **2003**, *37*, 1965–1968.
42. Vitry, V.; Bonin, L. Increase of boron content in electroless nickel-boron coating by modification of plating conditions. *Surf. Coat. Technol.* **2017**, *311*, 164–171. [CrossRef]
43. Lopez, J.R.; Mendez, P.F.; Perez-Bueno, J.J.; Trejo, G.; Stremsdoerfer, G.; Meas, Y. The effect of boron content, crystal structure, crystal size on the hardness and the corrosion resistance of electrodeposited Ni-B coatings. *Int. J. Electrochem. Sci.* **2016**, *11*, 4231–4244. [CrossRef]
44. Oraon, B.; Majumdar, G.; Ghosh, B. Improving hardness of electroless Ni-B coatings using optimized deposition conditions and annealing. *Mater. Des.* **2008**, *29*, 1412–1418. [CrossRef]
45. Krishnaveni, K.; Sankara Narayanan, T.S.N.; Seshadri, S.K. Electroless Ni-B coatings: Preparation and evaluation of hardness and wear resistance. *Surf. Coat. Technol.* **2005**, *190*, 115–121. [CrossRef]
46. Aydeniz, A.I.; Goksenli, A.; Dil, G.; Muhaffel, F.; Calli, C.; Yuksel, B. Electroless Ni-B-W coatings for improving hardness, wear and corrosion resistance. *Mater. Tehnol.* **2013**, *47*, 803–806.
47. Mukhopadhyay, A.; Barman, T.K.; Sahoo, P. Co-deposition of W and Mo in electroless Ni-B coating and its effect on the surface morphology, structure, and tribological behavior. *Proc. Inst. Mech. Eng. Part L J. Mater. Des. Appl.* **2021**, *235*, 149–161. [CrossRef]
48. Liu, H.; Viejo, F.; Guo, R.X.; Glenday, S.; Liu, Z. Microstructure and corrosion performance of laser-annealed electroless Ni-W-P coatings. *Surf. Coat. Technol.* **2010**, *204*, 1549–1555. [CrossRef]
49. Drovosekov, A.B.; Ivanov, M.V.; Krutskikh, V.M.; Lubnin, E.N.; Polukarov, Y.M. Chemically deposited Ni-W-B coatings: Composition, structure, and properties. *Prot. Met.* **2005**, *41*, 55–62. [CrossRef]
50. Biswas, P.; Kalyan Das, S.; Sahoo, P. Duplex electroless Ni-P/Ni-P-W coatings: Effect of heat treatment on tribological and corrosion performance. *Mater. Today Proc.* **2022**, *66*, 2237–2244. [CrossRef]
51. Estupinan, F.A.; Moreno, C.M.; Olaya, J.J.; Ardila, L.C. Wear Resistance of TiAlCrSiN Coatings Deposited by Means of the Co-Sputtering Technique. *Lubricants* **2021**, *9*, 64. [CrossRef]
52. Li, Z.; Farhat, Z.; Jarjoura, G.; Fayyad, E.; Abdullah, A.; Hassan, M. Synthesis and characterization of scratch-resistant Ni-P-Ti-based composite coating. *Tribol. Trans.* **2019**, *62*, 880–896. [CrossRef]
53. Balaraju, J.N.; Priyadarshi, A.; Kumar, V.; Manikandanath, N.T.; Kumar, P.P.; Ravisankar, B. Hardness and wear behaviour of electroless Ni-B coatings. *Mater. Sci. Technol.* **2016**, *32*, 1654–1665. [CrossRef]